ChemComm

Accepted Manuscript

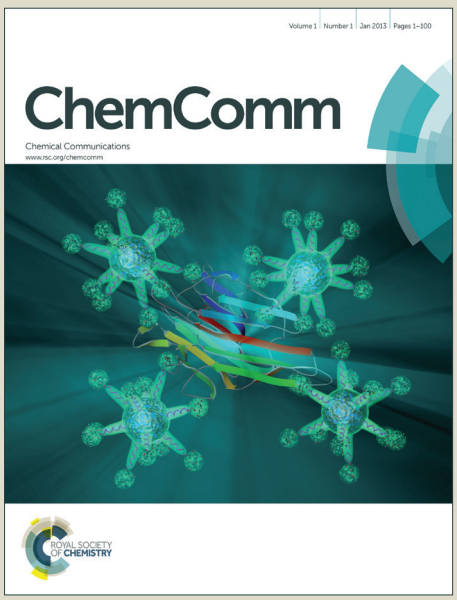

ROYAL SOCIETY OF CHEMISTRY

www.rsc.org/chemcomm

Cite this: DOI: 10.1039/c0xx00000x

www.rsc.org/xxxxxx

ARTICLE TYPE

$Sn@Ni_3Sn_4$ embedded in nanocable-like carbon hybrids for stable lithium-ion batteries

Xiaoyu Hou [a], Yanjie Hu*[a] , Hao Jiang [a], Yunfeng Li[a,b], Xiaofeng Niu [a] and Chunzhong Li*[a]

Received (in XXX, XXX) Xth XXXXXXXXX 20XX, Accepted Xth XXXXXXXXX 20XX

DOI: 10.1039/b000000x

Metallic $Sn@Ni_3Sn_4$ embedded in nanocable-like carbon hybrids have been successfully prepared by a novel gas-phase process, which exhibits a long cycle life (360 mA h g^{-1} at 1A g^{-1} after 1500 cycle) in lithium-ion batteries.

Lithium ion batteries (LIBs) with high energy and power density have been increasingly applied in the electric vehicles, energy storage systems.[1] A large number of anode materials with high capacity have been attracted and researched in order to replace the graphitic anode with limited capacity (372 mA h g^{-1}). Sn-based materials, alloying/delloying with lithium ions to acquire higher capacity (990 mA h g^{-1}), is one intriguing electrode material.[2] However, there still remain many challenges. For instance, Sn-based materials suffer from lithium-induced volume expansion/extraction, resulting in capacity loss and poor cycle life.[3]

A variety of strategies have been proposed to overcome the volume problem, which could be summarized into three categories, nanoscaling the materials, incorporation of other components and designing unique structure, such as hollow sphere, core-shell, or yolk-shell structure.[4-8] Tin-carbon system is regarded as an effective approach owing to advantages of low lost, facile synthesis route and excellent rate performance attributed by carbon component.[9-11] The carbon could work as buffering layer or matrix to restrict the volume change of Sn and improve the electrical conductivity of integrated electrode. For instance, Zhi et al. prepared tin-core/carbon-shell coaxial nanocables on reduced graphene electrode with 630 mA h g^{-1} for 50 cycle.[12] Our previously work reported an aerosol preparation of tin-catalysed Sn-filled CNTs architecture electrode with 437 mA h g^{-1} for 100 cycle.[13] Although the capacities are much higher than graphitic, the limited cycling life (≤100) is still a primary obstacle for further applications. The poor cycling performance is mainly assigned to the unsatisfactory mechanical stress of carbon layer and limited voids volume inside of carbon to suppress the volume expansion of tin. It is necessary to introduce other modified methods for improved cycling performance in the Sn/C electrode. Another strategy is to incorporate inactive metal M (such as Fe, Co, Ni, Sb) to synthesize intermetallic SnM, which M acts as electrochemically inactive matrix to release the volume change and mechanical stress as well as an electrical conductor[14,15]. Han et al. synthesized monodispersed MSn_5 (M=Fe, Co and FeCo) nanospheres with enhanced lithium storage compared to Sn.[16] However, the inactive metal M could only suppress part of volume expansion and the stress induced by lithium alloying/dealloying could not effectively eliminated, resulting in limited cycling life (most are less than 300 cycle).

Herein, $Sn@Ni_3Sn_4$ embedded in nanocable-like carbon hybrids have been successfully prepared by a novel gas-phase route, which combines the flame spray pyrolysis (FSP) process with chemical vapour deposition (CVD) process. The flame-made SnO_2/NiO nanoparticles were sintered into together and employed as catalysis for growing nanocable-like carbon in the CVD process. The introduced Ni component was extremely significant owing to the following two aspects. Firstly, phase-separation of Ni_3Sn_4 and Sn occurred where the former as intermetallic endowed the encapsulation layer with higher mechanical strength, releasing the stress induced by the volume change of Sn and preventing agglomeration and pulverization of Sn. Secondly, the catalytic activity of Ni_3Sn_4 was much higher than that of Sn, which could create more voids and vacancies in the interior of carbon layer, providing buffering space for tin-induced volume expansion. The as-obtained $Sn@Ni_3Sn_4$ embedded in nanocable-like carbon hybrids were employed as anode in LIBs and performed superior cycling stability and good rate performance.

The XRD pattern of as-prepared $Sn@Ni_3Sn_4$/C hybrids was displayed in the Fig. 1. The strong diffraction peaks indicated good crystallinity nature of the sample while it could be matched and indexed to metal Sn (PDF#65-2631) and intermetallic Ni_3Sn_4 (PDF#65-4553). The distinctive diffraction peaks of two phases Sn and Ni_3Sn_4 could be easily distinguished such as the (200) plane of Sn and the (111) plane of Ni_3Sn_4. In particular, the broaden peaks around 26 degree should be ascribed to the existence of carbon layer.

The morphology and detailed structure of $Sn@Ni_3Sn_4$/C hybrids s were demonstrated by field emission scanning electron microscopy (FESEM) as shown in the Fig. 2a and 2b. The obtained nanocables with diameter of 100-200 nm and length of 0.5-2 μm stacked and cross-linked into "flower-like" shape. During flame process, the SnO_2 and NiO nanocrystals underwent the nucleation, collision, coalescence and finally sintered into nanoaggregations owing to high flame temperature and rapidly quenching rate.[17,18] The schematic diagram of FSP route for preparation of SnO_2/NiO was shown in the Fig. S1, ESI. Notably, SnO_2/NiO existed as the form of aggregates and had the strong particle-particle interactions, not like the simple mixing of two separately nanoparticles. As shown in the Fig. S2 and S3, the

SnO_2 and NiO nanoparticles with average size of 10 nm were sintered into aggregates owing to unique aerosol flame process. During the CVD process, the C gases originated from C_2H_2 were catalysed by the SnO_2/NiO aggregates, eventually forming the "flower-like" nanocables hybrids.

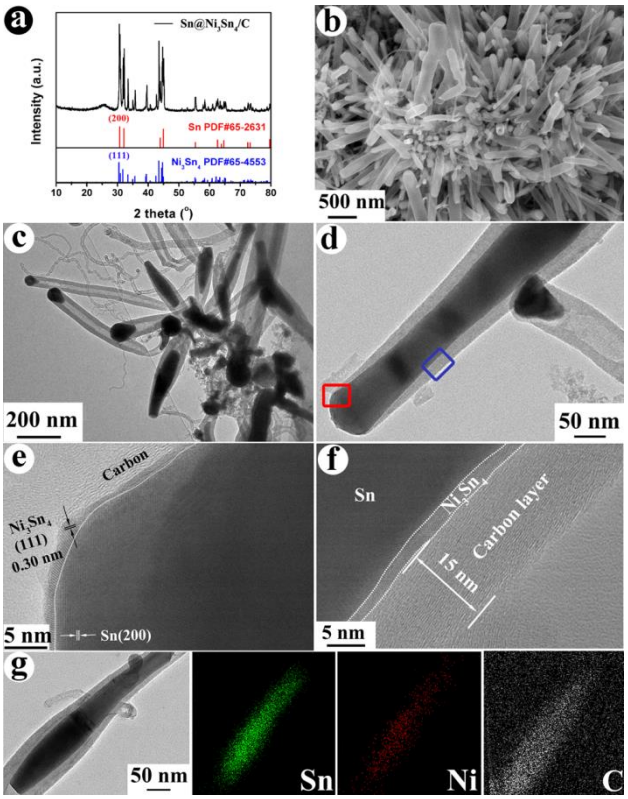

Fig. 1 (a) XRD pattern, (b) SEM image, (c, d) TEM images, (e, f) HRTEM, (g) TEM image and corresponding element mapping of as-obtained $Sn@Ni_3Sn_4$/C hybrids. (The Fig. 2e and 2f origin from the red and blue rectangles in Fig. 2d, respectively.)

More details of crystalline and structure could be obtained in the transmission electron microscopy (TEM), as shown in the Fig. 2c and 2d. Inner metals were clearly embedded inside the internal wall of nanocables carbon, judging from distinct contrasts in the TEM images. Interestingly, the carbon layer wrapped almost the entirety of the metals with a large portion of voids in the interior of nanocables. It was not negligible to observe the embedded volume of metals were quite different, which was mainly ascribed to the broaden size distribution of SnO_2/NiO nanoparticles. High resolution transmission electron microscopy (HRTEM) was characterized to further identify the structure and composition. Interestingly, Fig. 2e and 2f (magnified from the red and blue rectangles in the Fig. 2d) showed that the inter metals were constituted of core-shell structure. By means of measuring the lattice distance, core/shell composites with metal tin encapsulated by intermetallic Ni_3Sn_4 structure were affirmed. The 0.29 nm and 0.30 nm could be matched with (200) plane of Sn and (111) plane of Ni_3Sn_4, respectively. Besides, the carbon layers with thickness of about 15 nm were easily distinguished and wrapped on the surface of $Sn@Ni_3Sn_4$, forming the novel $Sn@Ni_3Sn_4$ embedded in nanocables carbon hybrids. The TEM along with elemental mapping (Fig. 2g) showed that Sn and Ni elements were uniformly distributed on the inner metals inside the nanocables while C element area was larger than that of Sn/Ni, which was well matched with the embedded structure between $Sn@Ni_3Sn_4$ and nanocables carbon. The selected area EDS affirmed that no trace of O was found, ensuring no existence of metal oxides (Fig S4a). The X-ray photoelectron spectroscopy (XPS) of $Sn@Ni_3Sn_4$/C hybrids were studied, further confirming the existence of Sn, Ni, C elements and the valence of Sn and Ni were 0 (484.7 eV for $3d_{5/2}$ of metal Sn, 852.2 eV for $2p_{3/2}$ of metal Ni), which was matched with metal state of Sn and intermetallic state of Ni_3Sn_4 (Fig. S4b). The carbon content of as-prepared sample was calculated to be 44.0% by the thermogravimetric analysis measurement (TGA) (Fig. S4c). Raman spectrum showed that the I(D)/I(G) was equal to 0.9, indicating nanocables carbon layers had many defects (Fig. S4d). Besides, the adsorption-desorption isotherms were carried out and the BET of $Sn@Ni_3Sn_4$/C hybrids was 36.1 m^2/g with a bimodal pore size distribution of 3.8 nm and 9.1 nm, respectively (Fig. S4e, f).

The growth mechanism of as-prepared $Sn@Ni_3Sn_4$/C hybrids in the CVD process was proposed in the Fig. 2a. The flame-synthesized SnO_2/NiO nanoparticles were firstly reduced into Sn/Ni metals by the gas C, which derived from decomposed C_2H_2 in the high temperature of 650 °C. As mentioned above, SnO_2/NiO nanoparticles were sintered with each other in the flame. Then the reduced Ni atoms began to dissolve in the molten Sn (melting point 231.9 °C) and they existed as solid solution. When more Ni dissolved into Sn and reached saturation state, the Ni trended to diffuse outwardly on the surface of tin, leading to diffused phase transition, forming a new intermetallic compound phase Ni_3Sn_4. Owing to the high temperature, the phase transformation diffusion processed rapidly and the phase-separation between Ni_3Sn_4 and Sn occurred, finally generating core/shell structure of $Sn@Ni_3Sn_4$. The decomposed C gas was constantly dissolved and deposited onto the molten $Sn@Ni_3Sn_4$. With catalysis assistance of $Sn@Ni_3Sn_4$, the carbons started to nucleate on the surface of $Sn@Ni_3Sn_4$ and grow in one specific direction, forming the $Sn@Ni_3Sn_4$ embedded in nanocable-like carbon hybrids. When the CVD process terminated and temperature cooled down, the molten $Sn@Ni_3Sn_4$ freezed and contracted, providing more voids volume in the interior of nanocables. The growth mechanism of $Sn@Ni_3Sn_4$/C hybrids was quite different from that of Sn@C nanowires, which was also displayed as comparison. As shown in Fig. 2b, the C gas was dissolved and grown on the root of molten Sn. Owing to the capillary action, the molten Sn filled into the interior of carbon nanowires. After the process of contraction, the limited voids were created in the top of each nanowire (TEM see Fig. S5a). In contrast, by the assistant of high efficient catalysis activity of Ni_3Sn_4, the carbon grown rapidly on the surface of $Sn@Ni_3Sn_4$, making the nanocables longer and supporting more voids in the interior of nanocables, which could provide more volume for tin-induced expansion (Fig. S5b). In addition, the appearance of Ni_3Sn_4 phase was mainly ascribed to sintered SnO_2/NiO nanoparticles. When SnO_2 and NiO nanoparticles were separately prepared by FSP and milled into together with same stoichiometric ratio as catalysis, the obtained composite was composed of tin-catalyzed Sn@C nanowires and nickel-catalysed CNTs (Fig. S5c), further indicating the flame-made SnO_2/NiO

with sintered particle-particle interactions was crucial for the preparation of Sn@Ni_3Sn_4/C hybrids. Moreover, the ratio of Sn/Ni in SnO_2/NiO could also affect the formation of Ni_3Sn_4. When the ratio changed to 1:1 in flame, the as-prepared sample after CVD were consisted of $Ni_{3.39}Sn_4$ and $Ni_{2.67}Sn_2$ alloys with more content of CNTs (TEM, XRD see Fig. S6).

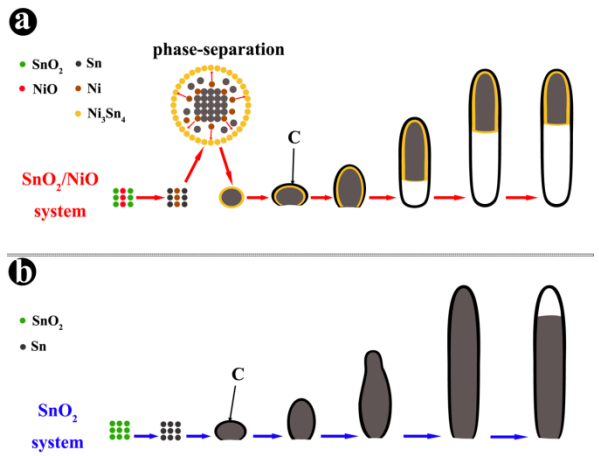

Fig. 2 Schematic growth mechanism of (a) Sn@Ni_3Sn_4/C hybrids and (b) Sn@C nanowires.

The Sn@Ni_3Sn_4/C hybrids electrode was assembled into 2016 coin cell to evaluate the lithium storage performance. Firstly, the cyclic voltammetry (CV) curve was performed to study the electrochemical reactions during the charge/discharge process (Fig. 3a). The initial cathodic sweep in the range from 0.5 to 1.0V was different from the following two scans, which was attributed to the formation of solid electrolyte interface (SEI). The reversible four peaks between 0.5-0.8 V in the anodic scans and two peaks between 0.4-0.7V in the cathodic scans could be ascribed to the de-intercalation reaction of Li_xSn ($x<4.4$) to Sn and intercalation reaction of Sn with lithium ions to Li_xSn, respectively.[19] The characteristic peaks of CV curve were completely matched with the Sn-based electrode, indicating the Ni content in the Ni_3Sn_4 was electrochemical inactive during the process.

The charge/discharge cycling was demonstrated to measure the reversible capacity of Sn@Ni_3Sn_4/C hybrids electrode (Fig. 3b). As comparison, the Sn@C nanowires without Ni_3Sn_4 layer and flame-made SnO_2/NiO nanoparticles were also assembled into cells (TEM of Sn@C nanowires see Fig. S5a, cycle performance of SnO_2/NiO see Fig. S7). The discharge-charge voltage profiles were shown in the Fig. S8. The initial discharge capacity of Sn@Ni_3Sn_4/C hybrids electrode (564 mA h g^{-1}) was lower than that of Sn@C electrode (654 mA h g^{-1}) while the capacity increased to above 410 mA h g^{-1} after 800 cycles even though a transitory decline of capacity was found before 50 cycles. By comparison, the Sn@C nanowires without protection of Ni_3Sn_4 decreased swiftly below 100 mA h g^{-1} after 60 cycles. From this point, the introduction of Ni_3Sn_4 decreased the theoretical capacity of the Sn-based electrode while prolonged the cycling life tremendously. Moreover, the CV curve of the cell after 800 cycles had been tested to identify the electrochemical process after cycling, as shown in the Fig. S9. Two separated broaden peaks around 0.4-0.7 V and 1.1-1.3 V were ascribed to characteristic peaks of deintercalation of Li_xSn and Li_yC, repectively, revealing that the capacity was still attributed by Sn and carbon layer.

The rate performance of Sn@Ni_3Sn_4/C hybrids electrode was evaluated by varying the current density from 0.2 A g^{-1} to 2 A g^{-1} gradually. The capacity dropped before 40 cycles and remained 343 mA h g^{-1}, 275 mA h g^{-1}, 248 mA h g^{-1}, 220 mA h g^{-1}, 281 mA h g^{-1} when the current density was 0.2 A g^{-1}, 0.5 A g^{-1}, 1 A g^{-1}, 2 A g^{-1}, 0.2 A g^{-1}, respectively, revealing the capacity decreased slightly with rapidly increasing currents. To further understanding the electrochemical process during the charge/discharge cycling, the nyquist plots of Sn@Ni_3Sn_4/C hybrids electrode were carried out to measure the electrochemical impedance spectroscopy (EIS) (Fig. 3d). The EIS curves of three coins (after CV scans, after 50 cycles, after 800 cycles, respectively) were consisted of two semi-circles and a linear line, representing the bulk resistance of the cell R_e, resistance of SEI on the surface of two electrodes R_{sei}, charge-transfer resistance R_{ct}, respectively.[20] It can be observed that the resistance of R_e reduced continuously along with increasing cycling. Simultaneously, the R_{sei} for 50 cycles (78.3 Ω) was much larger than that of 800 cycles (29.1 Ω). This phenomenon might origin from the activation process between electrode and the electrolyte after increasing cycling. The cycling life of Sn@Ni_3Sn_4/C hybrids electrode was tested by charge/discharge cycling with 1 A g^{-1} current density (Fig. 3e). Similarly, the capacity dropped before 50 cycles and increased gradually to 360 mA h g^{-1} after 1500 cycles. The outstanding cycling stability for 1500 cycles of Sn@Ni_3Sn_4/C electrode was mainly attributed to the hybrids structure with two protections of carbon layers and Ni_3Sn_4 layers with more voids in the interior of nanocables.

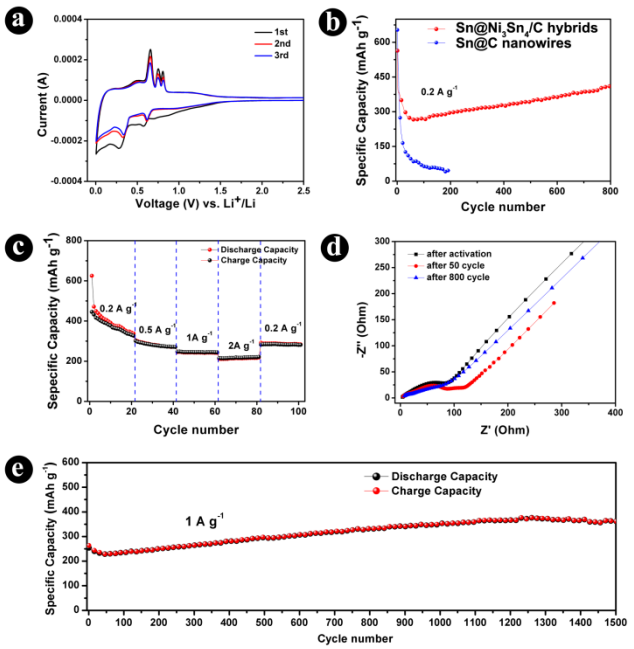

Fig. 3 (a) CV profile at a voltage range from 0.005 to 3V at the scanning rate of 0.2 mVs^{-1}, (b) cycling charge/dsicharge in the current density of 0.2 A g^{-1}, (c) rates capacity performance varying from 0.2 A g^{-1} to 2 A g^{-1}, (d) Nyquist plots of cells under frequence range of 0.01 to 10^5 Hz, (e) cycling performance with 1 A g^{-1} of Sn@Ni_3Sn_4/C hybrids electrode.

The ex-situ TEM was characterized to analyse the structure

variations of the electrode during the cycling process. Fig 4a,b,c,d represented the structure of Sn@Ni_3Sn_4/C hybrids after 50 cycle, 100 cycle, 800 cycle and 1500 cycle, respectively. The Sn@Ni_3Sn_4 was completely restricted in the interior of carbons before 100 cycles. The existence of Ni_3Sn_4 and carbon layers with mechanical strength suppressed the volume expansion of Sn and the voids inside the nanocables also relieved the tin-induced stress. The reason for the decreasing capacity before 50 cycles could be ascribed to the side reactions of electrolyte and lack wettability between electrode and electrolyte, which was proved by larger R_{sei} in the EIS for 50 cycles. When the charge/discharge cycling proceeded as long as 800 cycles, most of Sn@Ni_3Sn_4 were still embedded inside of carbon layers while the carbon layers cross-linked into together, indicating an excellent conductivity of integral electrode. Meanwhile, most of the metal Sn was still confined inside the nanocables, confirming that carbon and Ni_3Sn_4 layers played an important role on sustaining the superior cycling stability. When the cycling number increased to 1500 cycle, some of Sn aggregated into together, explaining a little decline of the reversible capacity after 1300 cycle.

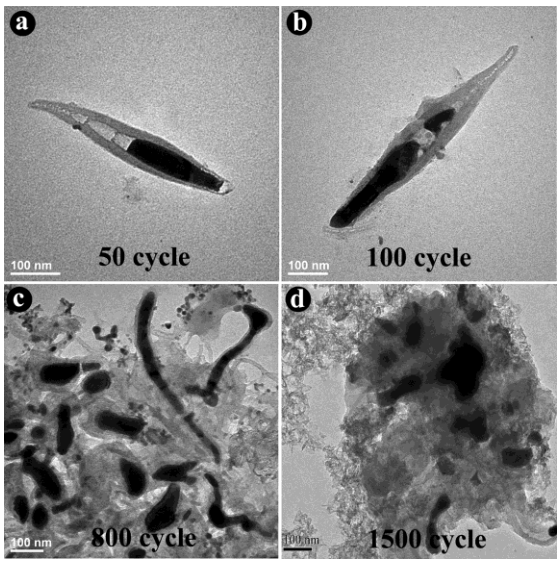

Fig. 4 TEM images of Sn@Ni_3Sn_4/C hybrids electrode after constant-current charge-dicharge cyclings, (a) 50 cycle, (b) 100 cycle, (c) 800 cycle and (d) 1500 cycle.

In summary, we have successfully synthesized Sn@Ni_3Sn_4 embedded in nanocable-like carbon hybrids. The unique structure with confinement of Sn in the inferior of nanocables by carbon and Ni_3Sn_4 layers, more voids in the interior of nanocables and superior electron conductivity, relieved the volume change and stress during the Li_xSn alloying/dealloying processes, preforming outstanding cycling stability and remaining above 360 mA h g^{-1} after 1500 cycles.

This work was supported by the National Natural Science Foundation of China (21322607, 21371057), the Basic Research Program of Shanghai (14JC1490700), the Special Research Fund for the Doctoral Program of Higher Education of China (20120074120004), the Research Project of Chinese Ministry of Education (113026A), Project funded by China Postdoctoral Science Foundation (2014M561497) and the Fundamental Research Funds for the Central Universities.

Notes and references

[a] *Key Laboratory for Ultrafine Materials of Ministry of Education, School of Materials Science and Engineering, East China University of Science and Technology, Shanghai 200237, China. Fax: +86 21 6425 0624; Tel: +86 21 6425 0949; E-mail: czli@ecust.edu.cn ; huyanjie@ecust.edu.cn*
[b] *Shanghai Nanotechnology Promotion Center, Shanghai 200237, China*

† Electronic Supplementary Information (ESI) available: [Schemtic diagram of FSP, TEM, XRD cycle performance of flame-made SnO_2/NiO, TEM, EDS, XPS, TGA, Raman, BET, pore size distribution of Sn@Ni_3Sn_4/C hybrids, charge/discharge *vs.* voltage profiles, CV curve after 800 cycles of Sn@Ni_3Sn_4/C hybrids electrode, TEM, XRD of contrast sample]. See DOI: 10.1039/b000000x/

1 N. S. Choi, Z. Chen, S. A. Freunberger, X. Ji, Y. K. Sun, K. Amine, G. Yushin, L. F. Nazar, J. Cho and P. G. Bruce, *Angew. Chem., Int. Ed*., 2012, **51**, 9994.
2 I. A. Courtney and J. R. Dahn, J. Electrochem. Soc., 1997, 144, 2045.
3 Y. Xu, Q. Liu, Y. Zhu, Y. Liu, A. Langrock, M. R. Zachariah and C. Wang, *Nano Lett*., 2013, **13**, 470.
4 W. J. Zhang, *J. Power Sources*, 2011, **196**, 13.
5 Z. Y. Wang, L. Zhou and X. W. Lou, *Adv. Mater*., 2012, **24**, 1903.
6 C. Guan, X. H. Wang, Q. Zhang, Z. X. Fan, H. Zhang and H. J. Fan, *Nano Lett*., 2014, **14**, 4852.
7 W. Ni, Y. B. Wang and R. Xu, *Part. Part. Syst. Charact.* 2013, **30**, 873.
8 J. Z. Chen, L. Yang, Z. X. Zhang, S. H. Fang and S. I. Hirano, *Chem. Commun*., 2013, **49**, 2792.
9 J. Hassoun, G. Derrien, S. Panero and B. Scrisati, *Adv. Mater*., 2008, **20**, 3169.
10 Y. Q. Zou and Y. Wang, *ACS nano*, **5**, 2011,8108.
11 A. Jahel, C. M. Ghimbeu, L. Monconduit and C. Vix-Guterl, *Adv. Energy Mater*., 2014, **4**, 1400025.
12 B. Luo, B. Wang, M. H. Liang, J. Ning, X. L. Li and L. J. Zhi, *Adv. Mater*., 2012, **24**, 1405.
13 X. Y. Hou, H. Jiang, Y. J. Hu, Y. F. Li, J. C. Huo and C. Z. Li, *ACS Appl. Mater. Interfaces.* 2013, 5, 6672.
14 M. Chamas, M. T. Sougrati, C. Reibel and P. E. Lippens, *Chem. Mater*., 2013, **25**, 2410.
15 Y. Gu, F. Wu and Y. Wang, *Adv. Funct. Mater*., 2013, **23**, 893.
16 F. X. Xin, X. L. Wang, J. M. Bai, W. Wen, H. J. Tian, C. S. Wang and W. Q. Han, *J. Mater. Chem. A*, 2015, **3**, 7170.
17 R. Strobel and S. E. Pratsinis, *J. Mater. Chem.*, 2007, **17**, 4743.
18 X. Y. Hou, Y. J. Hu, H. Jiang, Y. F. Li, W. G. Li and C. Z. Li, *J. Mater. Chem. A*, 2015, **3**, 9982.
19 D. Deng and J. Y. Lee, *Angew. Chem., Int. Ed.*, 2009, **48**, 1660.
20 S. S. Zhang, K. Xu and T. R. Jow, *Eletrochimica Acta*, 2006, **51**, 1636.

A graphical abstract for the contents page

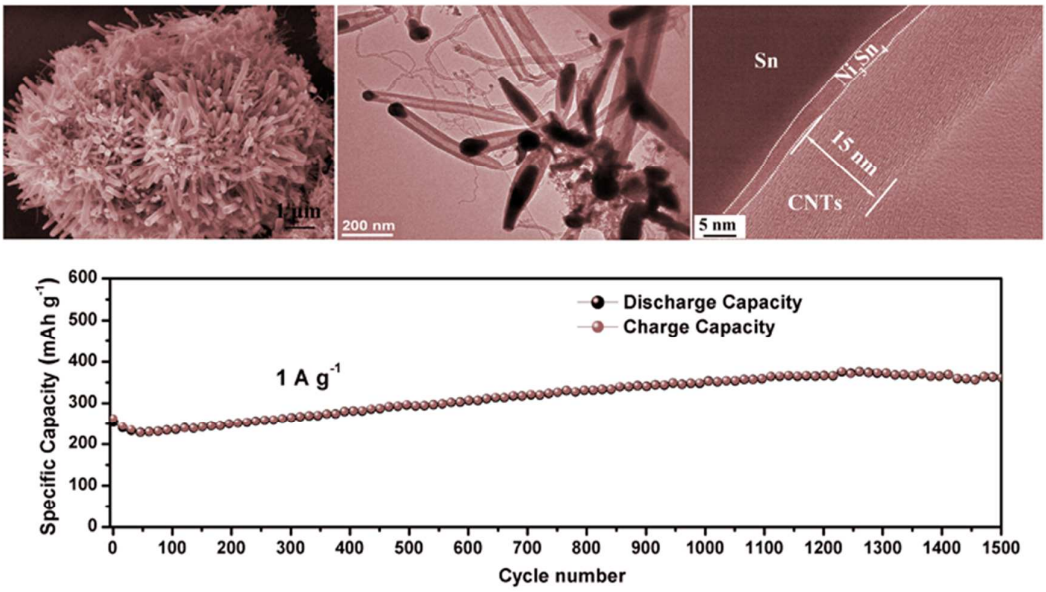

$Sn@Ni_3Sn_4$ embedded in nanocable-like carbon hybrids have been successfully prepared by a novel gas-phase route. The introduced Ni_3Sn_4 layer not only suppresses the tin-induced volume expansion, but also provides more voids and vacancies in the interior of nanocables. When used as anode in LIBs, the $Sn@Ni_3Sn_4$/C hybrids exhibits a long cycle life (360 mA h g^{-1} at 1A g^{-1} after 1500 cycle).